ACS APPLIED MATERIALS & INTERFACES

Research Article

Cite This: ACS Appl. Mater. Interfaces 2019, 11, 33770−33780

www.acsami.org

Interfacial Engineering for High-Efficiency Nanorod Array-Structured Perovskite Solar Cells

Bingbing Cao,[†] Haoran Liu,[†] Longkai Yang,[†] Xin Li,[*,†] Hu Liu,[‡,§] Pei Dong,[⊥] Xianmin Mai,[*,#] Chuanxin Hou,[▽] Ning Wang,[∥] Jiaoxia Zhang,[§,○] Jincheng Fan,[◆] Qiang Gao,[*,¶] and Zhanhu Guo[*,§]

[†]Pen-Tung Sah Institute of Micro-Nano Science and Technology, Xiamen University, Xiamen 361005, China

[‡]Key Laboratory of Materials Processing and Mold (Zhengzhou University), Ministry of Education; National Engineering Research Center for Advanced Polymer Processing Technology, Zhengzhou University, Zhengzhou 450002, China

[§]Integrated Composites Laboratory (ICL), Department of Chemical & Biomolecular Engineering, University of Tennessee, Knoxville, Tennessee 37996, United States

[∥]State Key Laboratory of Marine Resource Utilization in South China Sea, Hainan University, Haikou 570228, China

[⊥]Department of Mechanical Engineering, George Mason University, Fairfax, Virginia 22030, United States

[#]School of Urban Planning and Architecture, Southwest Minzu University, Chengdu 610041, China

[▽]School of Materials Science and Engineering, North University of China, Taiyuan 030051, China

[○]School of Materials Science and Engineering, Jiangsu University of Science and Technology, Zhenjiang 212003, China

[◆]College of Materials Science and Engineering, Changsha University of Science and Technology, Changsha 410114, China

[¶]Scanning Probe Microscopy Group, Center for Nanophase Materials Sciences, Oak Ridge National Laboratory, PO Box 2008, Oak Ridge, Tennessee 37831, United States

Supporting Information

ABSTRACT: TiO_2 nanorod (NR) array for perovskite solar cells (PSCs) has attained great importance due to its superb power conversion efficiency (PCE) compared to that of the traditional mesoporous TiO_2 film. A TiO_2 compact layer for the growth of TiO_2 NR array via spin-coating cannot meet the requirements for efficient NR-based PSCs. Herein, we have developed and demonstrated the insertion of a bifunctional extrathin TiO_2 interlayer (5 nm) by atomic layer deposition (ALD) at the interface of the fluorine-doped tin oxide (FTO)/TiO_2 compact layer to achieve alleviated electron exchange and a reduced energetic barrier. Thus, an accelerated extraction of electrons from TiO_2 NR arrays via the compact layer and their transfer to the FTO substrate can improve the PSC efficiency. The thickness of the spin-coated TiO_2 compact layer on the ALD-deposited TiO_2 layer is spontaneously optimized. Finally, an outstanding efficiency of 20.28% has been achieved from a champion PSC with negligible hysteresis and high reliability. To the best of our knowledge, this is the first study demonstrating the superiority of TiO_2-NR-based PSCs withstanding the dry heat and thermal cycling tests. The results are of great importance for the preparation of efficient and durable PSCs for real-world applications.

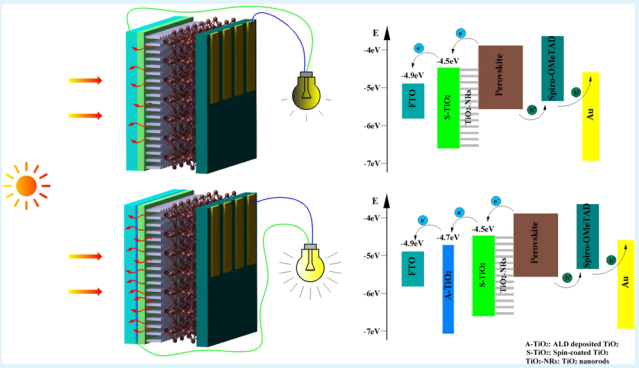

KEYWORDS: *TiO_2 nanorod, perovskite solar cells, atomic layer deposition, compact layer, depletion region*

INTRODUCTION

Perovskite solar cells (PSCs) have attracted intensive attention because of unexpected solution processability at low temperatures and ever-increasing power conversion efficiency (PCE).[1] Since the pioneering work in 2009,[2] the PCE has been dramatically improved via compositional engineering,[3,4] passivating the interface,[5,6] and kinds of carrier transporting materials.[7,8] Organic−inorganic halide perovskites (OIHPs) have been recognized as one of the most promising materials for PSCs, owing to their excellent light absorption, large electron/hole diffusion lengths, and good solution processability.[9] Generally, PSCs present a layered sandwiched structure including an electron transport layer (ETL), a perovskite absorber layer, and an organic hole transport layer (HTL).[10] Two main kinds of ETL structures exist including a planar structure and a TiO_2 mesoporous structure. Although

Received: May 1, 2019
Accepted: August 1, 2019
Published: August 1, 2019

DOI: 10.1021/acsami.9b07610
ACS Appl. Mater. Interfaces 2019, 11, 33770−33780

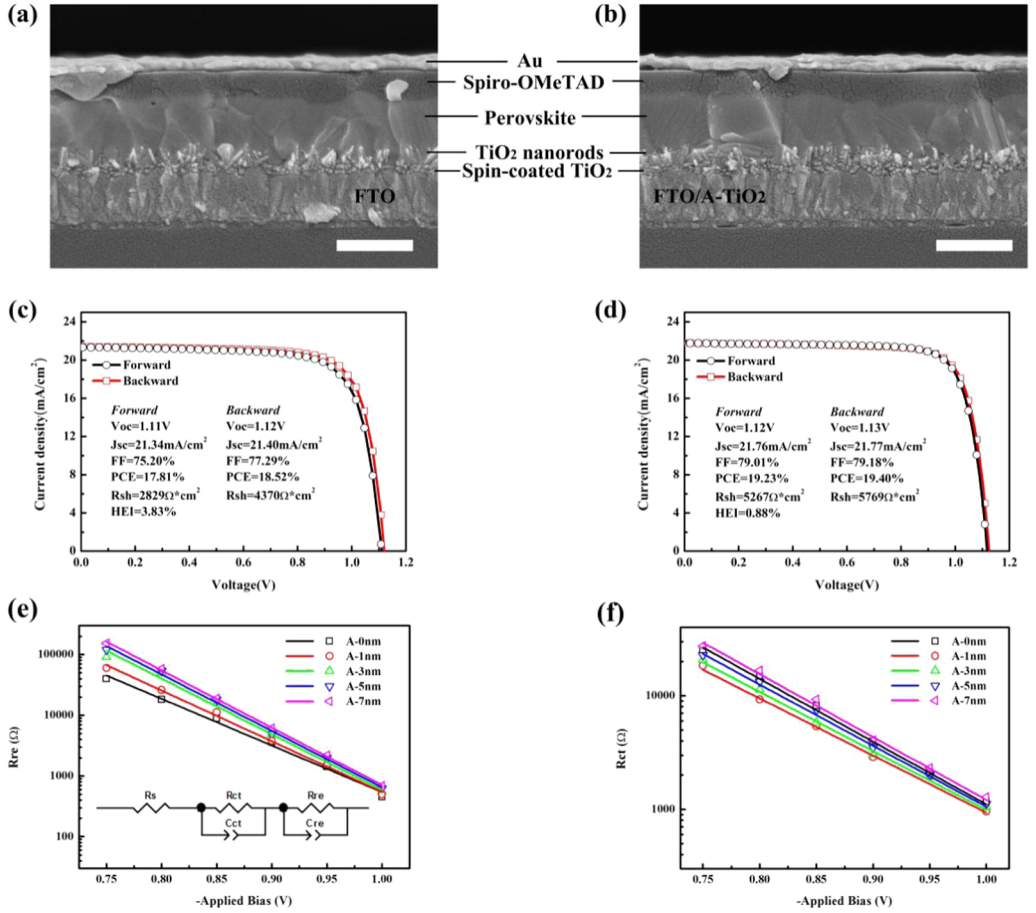

Figure 1. Cross-sectional SEM images of PSCs (a) without and (b) with the A-TiO_2 interlayer. Current density/voltage (J–V) curves of PSCs (c) without and (d) with the A-TiO_2 extrathin layer (5 nm). (e) Recombination resistance (R_{re}) and (f) charge transfer resistance (R_{ct}) extracted from fitted electrochemical impedance spectra of perovskite solar cells at different applied biases. The perovskite solar cells with A-TiO_2 thicknesses of 0, 1, 3, 5, and 7 nm were denoted A-0 nm, A-1 nm, A-3 nm, A-5 nm, and A-7 nm, respectively. The thickness of the S-TiO_2 layer is 65 nm.

outstanding efficiencies have been achieved on planar-structured ETLs, e.g., SnO_2,[11,12] the different thermal expansion coefficients of the planar metal oxide ETLs and the perovskite layers result in stress in the perovskite films and cause delamination, the same as the PSCs under outdoor temperature cycling.[9,13] In contrast, PSCs based on mesoporous ETLs withstand severe temperature cycling owing to the penetration of the ETLs into the perovskite films.[14,15] Thus, intensive works have been focused on the modification or replacements of the typical TiO_2-based mesoporous ETLs to improve the PSC performance. Peng et al. modified compact TiO_2/mesoporous TiO_2 using a PMMA:PCBM mixture and achieved an efficiency of up to 20.4% without any hysteresis.[6] Seok et al. prepared $BaSnO_3$:La using a solution route as ETLs and attained an efficiency as high as 21.2%.[8] Doping of elements into TiO_2 has demonstrated improved efficiency and stability of PSCs as well.[16−19]

One-dimensional (1D) metal oxide films, such as TiO_2 nanorod (NR) or nanotube (NT) array films, are much appreciated among high-performance ETLs nowadays, owing to their uniquely ordered structures. They have been applied in many electronic devices, for example, solid-state dye-sensitized solar cells (SSDSCs),[20] sensors,[21] and betavoltaics,[22] where fast electron transportation within the ETL and effective electron extraction at the ETL/charge-selective contact interface are required. Recently, TiO_2 NR or NT arrays have also been intensively studied in PSCs,[23−26] exhibiting higher electron mobility, longer diffusion length, and improved pore filling compared to those of nanoparticle-based mesoporous structures.[27−32] In a recent report, Cui et al. have achieved an efficiency of up to 19.11% by doping Ta into TiO_2 NRs to modify the band alignment, which is one of the highest efficiencies for PSCs based on TiO_2 NRs.[33]

Although great progress has been made for boosting PCE of these PSCs based on 1D oriented nanostructures, further enhancement remains challenging. Interfacial engineering is well known to be an important way to improve the PCE through enhancing charge collection and reducing charge recombination.[6,34,35] Of all of the interfaces within the PSCs, the fluorine-doped tin oxide (FTO)/ETL interface is of vital importance.[36−40] Spin-coating, spray pyrolysis, and ALD are the most common routes to fabricate high-quality compact ETLs. Previously, the film fabricated by atomic layer deposition (ALD) has been claimed to possess the lowest pinhole density and suppress the recombination of charges.[39,41] Nevertheless, interfacial modification was still required to modify the FTO/ETL interface to enhance the PCE. It has been demonstrated to use double-layer, n-type compact layers to obtain sufficient electron extraction, including the combination of metal oxide/PCBM,[42,43] TiO_2/SnO_2,[44] and ZnO/SnO_2.[45] Most of these studies focused on planar-ETL-based PSCs, and there are a few reports that

DOI: 10.1021/acsami.9b07610
ACS Appl. Mater. Interfaces 2019, 11, 33770−33780

Table 1. Summary of Photovoltaic Parameters of Perovskite Solar Cells Based on Different Combinations of TiO_2 ETLs[a]

ETL combination (10 average)	V_{oc} (V)	J_{sc} (mA/cm^2)	FF (%)	PCE (%)
A-TiO_2	1.07 ± 0.01	21.33 ± 0.23	64.42 ± 4.60	14.65 ± 1.15
S-TiO_2	1.04 ± 0.02	21.24 ± 0.23	66.27 ± 3.53	14.59 ± 1.11
S-TiO_2/mesoporous TiO_2	1.11 ± 0.01	21.68 ± 0.16	77.29 ± 1.39	18.65 ± 0.54
A-TiO_2/TiO_2 NR	1.08 ± 0.02	21.44 ± 0.16	71.38 ± 2.22	16.55 ± 0.72
S-TiO_2/TiO_2 NR	1.11 ± 0.01	21.23 ± 0.15	76.37 ± 1.10	17.95 ± 0.49
A-TiO_2/S-TiO_2/TiO_2 NR	1.12 ± 0.01	21.77 ± 0.11	78.20 ± 0.66	18.99 ± 0.25

[a]The thicknesses of the A-TiO_2 layer and S-TiO_2 layer are 5 and 65 nm, respectively.

pinpoint the effect of the FTO/1D oriented ETL (especially the TiO_2-NR-array film) interface toward achieving high PCEs. Although the compact TiO_2 underlayer as the seeding layer for the growth of the TiO_2 NR array can act as an interfacial layer between the FTO and TiO_2-NR-array ETL,[46−53] significant issues remain for the compact layer/TiO_2-NR-array architecture such as interfacial charge extraction and band alignment. It is thus very significant to tailor the seeding layer under NR arrays to enhance electron extraction and collection.[33]

In this work, we have demonstrated a novel methodology employing an extrathin TiO_2 layer by ALD to modify the interface between FTO and the seeding layer of TiO_2 NR arrays. The introduction of the extrathin interlayer gave a TiO_2 compact layer (seeding layer) having reduced surface-energy difference and better lattice matching. The extrathin layer has enhanced the electron extraction by offering a space barrier against charge recombination and a better energy-level alignment between FTO and the TiO_2 compact layer. The thickness of the TiO_2 compact layer, which could cause charge accumulation at the TiO_2/FTO interface and slow electron transportation,[38,54] has been examined to obtain an optimal thickness for efficient PSCs. By employing the optimized FTO/ALD-TiO_2/TiO_2 compact layer structure, a PCE as high as 20.28% for TiO_2-nanorod-structured PSCs has been achieved with long-term reliability under dry heat and thermal cycling conditions.

RESULTS AND DISCUSSION

The typical TiO_2 NR array-based anode is presented in Figure S1 of the Supporting Information, where it is prepared on a TiO_2 seeding layer as the oriented scaffold for depositing the perovskite active layer. The TiO_2 NR array film has a thickness of ∼180 nm with a nanorod diameter of ∼30 nm. The dense TiO_2 thin layer is prepared via the spin-coating method and has a thickness of approximately 65 nm (spin-coated TiO_2 compact layer, denoted S-TiO_2). In such a way, photon-induced electrons within the perovskite active layer can be effectively extracted and then transferred to the FTO substrate by the dense TiO_2 layer. According to the ultrafast electron transport within TiO_2 NRs,[55] the dense TiO_2 layer plays a substantial role in collecting the electrons injected by the FTO substrates. The electrons within the compact layer must be transferred as quickly as possible to avoid charge accumulation and meanwhile to prevent the recombination between the electrons and the holes in the perovskites. There are inevitable pinholes existing within the spin-coated dense film, possibly leading to recombination losses.[38] In this work, the defects within the spin-coated film can be remedied by inserting an extrathin interlayer between FTO and the dense film (Figure S1b, SI). To deposit the extrathin layer, we have employed ALD in a controlled manner. The resulting ALD-deposited thin layer (denoted A-TiO_2) enabled the targeted modification of the interface of the FTO/S-TiO_2 layer, and then, it allowed blocking of the negative pathways throughout the spin-coated TiO_2 compact layer. A similar morphology of the TiO_2 NR arrays on the S-TiO_2 layer and the S-TiO_2@A-TiO_2 layer has been recorded (Figure S1c,d, SI), indicating that the insertion of the A-TiO_2 layer is too thin to affect the growth of the TiO_2 NRs. We also tried to prepare the TiO_2 NR film directly onto the FTO/A-TiO_2 surface, as shown in Figure S2. The growing orientation of the TiO_2 NRs distributes randomly, which might impair the following penetration of the perovskite film and thus the PSC performance.

To evaluate the effect of the A-TiO_2 layer, PSC devices with quadruple-cation perovskite $K_{0.05}Cs_{0.05}(MA_{0.17}FA_{0.83})_{0.9}Pb(I_{0.83}Br_{0.17})_3$ as a light absorber have been fabricated by a one-step method with antisolvent quenching. The effect of the insertion of the A-TiO_2 film on the perovskite layer, HTL (spiro-OMeTAD), and Au layer has been examined by cross-sectional scanning electron microscopy (SEM, Figure 1a,b). For comparison, a A-TiO_2 interlayer (5 nm) was used, where no obvious difference was observed. Thus, A-TiO_2 would be responsible for the change of photovoltaic performance. To elucidate the thickness dependence of A-TiO_2, thicknesses of 1, 3, 5, and 7 nm of the A-TiO_2 layer were applied, and the photovoltaic parameters are presented in Table S1 of the Supporting Information. The thickness of the A-TiO_2 was determined, as shown in Figure S3. PSCs with different combinations of TiO_2 ETL are also given in Table 1. Obviously, PSCs with a combination of A-TiO_2/S-TiO_2/TiO_2 NR present a higher PCE value, especially when the thickness of the A-TiO_2 layer is 5 nm. We only focus on TiO_2-NR-based PSCs without the A-TiO_2 layer here. The short-circuit current density (J_{sc}) shows a slight increase on these A-TiO_2 containing devices, and the fill factor (FF) is greatly improved. Considering the similar open-circuit voltage (V_{oc}) values, the improved PCE can be attributed to the enhanced FF. Normally, the serial resistance and the recombination within a PSC account mainly for the change of FF. In our case, the perovskite layer, metal electrode, and FTO substrate remains unchnaged. Hence, the improved FF depends mainly on the reduced recombination. The shunt resistance (R_{sh}) of the two cells, which can reflect the recombination within the device simply, is extracted (Figure 1c,d). The R_{sh} is greatly increased by 30% upon insertion of the A-TiO_2 interlayer, thereby underpinning the fact that the A-TiO_2 layer reduced the recombination.

To further unravel the interfacial charge transfer and recombination processes, electrochemical impedance spectroscopy (EIS, Figure S4) spectra were recorded at different bias voltages with varied A-TiO_2 thicknesses. Through fitting the EIS data with an equivalent circuit (inset of Figure 1e), the values of series resistance (R_s), recombination resistance (R_{re}), recombination capacitance (C_{re}), and charge transfer resistance

DOI: 10.1021/acsami.9b07610
ACS Appl. Mater. Interfaces 2019, 11, 33770−33780

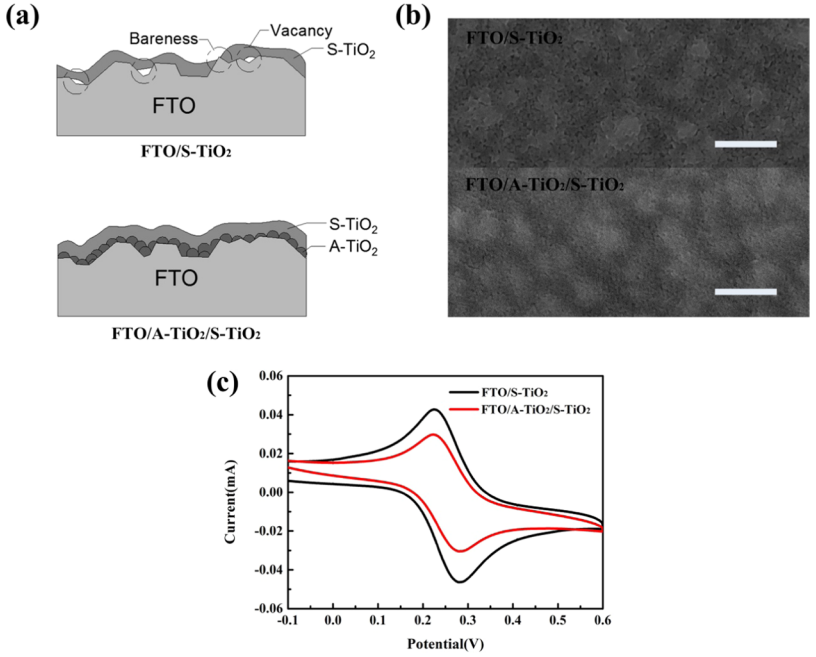

Figure 2. (a) Schematic drawings of the FTO/S-TiO_2 combination and the FTO/A-TiO_2/S-TiO_2 combination. (b) SEM images of S-TiO_2 on FTO and modified FTO by A-TiO_2; scale bar is 500 nm. (c) Cyclic voltammetry curves for FTO/S-TiO_2 and FTO/A-TiO_2(5 nm)/S-TiO_2 (65 nm).

at the ETL/perovskite interface or perovskite/HTL interface (R_{ct}) have been determined. The R_{re} decreases exponentially with the increase of applied bias (Figure 1e), owing to the exponential change of the TiO_2 surface states with the bias voltage. The R_{rec} increases with the insertion of the A-TiO_2 layer, indicating the effectively reduced recombination. Compared to the R_{ct} of the control device, the R_{ct} of A-TiO_2-containing devices decreases when the thickness of A-TiO_2 is below 7 nm (Figure 1f), indicating that the A-TiO_2 enhanced charge collection between the FTO substrate and perovskite layer. Thus, the improved performance of the PSCs by the insertion of A-TiO_2 arises from the reduced charge recombination and improved charge collection.

The morphological changes of the S-TiO_2 on the FTO substrates by the insertion of A-TiO_2 were examined by atomic force microscopy (AFM, Figure S5). The pristine FTO surface possesses a relative rough and a polyhedron composed morphology with a root-mean-square (RMS) roughness of 14.86 nm. After depositing the S-TiO_2 layer, the surface becomes flat with an RMS of 5.60 nm. Upon adding the A-TiO_2 layer between FTO and the S-TiO_2 layer, the FTO surface became flat with an RMS of 7.01 nm, showing a spherelike morphology from the uniformly deposited TiO_2 film by ALD. As a result, the S-TiO_2 layer surface becomes flat with an RMS roughness of 4.41 nm, which was lower than that of the S-TiO_2 on pristine FTO. The improved homogeneity of the S-TiO_2 layer originated from the flatter surface of FTO with A-TiO_2.[56]

Another beneficial effect of inserting the A-TiO_2 layer would be to reduce the physical defects at the FTO/S-TiO_2 interface. The voids between FTO crystals and the S-TiO_2 layer, thin TiO_2 layers atop the protruding FTO crystals, and thick TiO_2 layers between FTO crystals are regarded as contact defects and cannot be eliminated by the spin-coated sol−gel process. The schematic figure is shown in Figure 2a. These defects may originate from the surface energies of the FTO and TiO_2, and the volume shrinkage of the TiO_2 film,[57] and might increase the electron/hole recombination between the electrons in FTO and the holes at the S-TiO_2 surface. When using the A-TiO_2 layer, the S-TiO_2 was deposited on the A-TiO_2 directly, suggesting that the surface-energy difference became much less than that of the FTO/S-TiO_2. Thus, the defects between the FTO and S-TiO_2 have been reduced greatly. The existence of A-TiO_2 enables a natural space barrier to block the recombination through the FTO/S-TiO_2 interface. On the other hand, the pinhole density within the compact layer has been decreased by introducing the A-TiO_2 layer (Figure 2b). The pinhole density and diameter of the S-TiO_2 layer on FTO/A-TiO_2 were much lower than those of the S-TiO_2 layer on bare FTO. A previous study indicated that the pinhole density within the compact layer for photoelectrochemical devices can affect the charge exchange between the FTO and electrolyte effectively.[58] Hence, the decreased pinhole density would contribute to the reduced recombination crossing FTO/S-TiO_2 simultaneously. The morphologies of the two S-TiO_2 layers are different, and hence, Raman spectroscopy has been utilized to detect TiO_2 crystallized locally in the S-TiO_2 layers on FTO and FTO/A-TiO_2 (Figure S6). A-TiO_2 on FTO was measured for references at the same time. For the A-TiO_2 film, no obvious signal can be detected, ascribed to the thickness of only 5 nm. XRD measurements showed that the as-prepared A-TiO_2 belongs to amorphous TiO_2 (Figure S6). However, the amorphous A-TiO_2 is turned into anatase phase when the S-TiO_2 is deposited on FTO/A-TiO_2 and then annealed at 450 °C for the further growth of the TiO_2 NR array (Figure S6). For the FTO/S-TiO_2 sample, the low-frequency E_g around 145 cm^{-1} was produced owing to the external vibration of the lattice for anatase TiO_2.[59] Regarding the FTO/A-TiO_2/S-TiO_2, a blue shift of the scattering band can be ascribed to a better crystallinity of TiO_2 in the S-TiO_2 layer.[38] The enhanced crystallinity of TiO_2 suggests the less trap states, which is of interest to reduce the recombination. The

DOI: 10.1021/acsami.9b07610
ACS Appl. Mater. Interfaces 2019, 11, 33770−33780

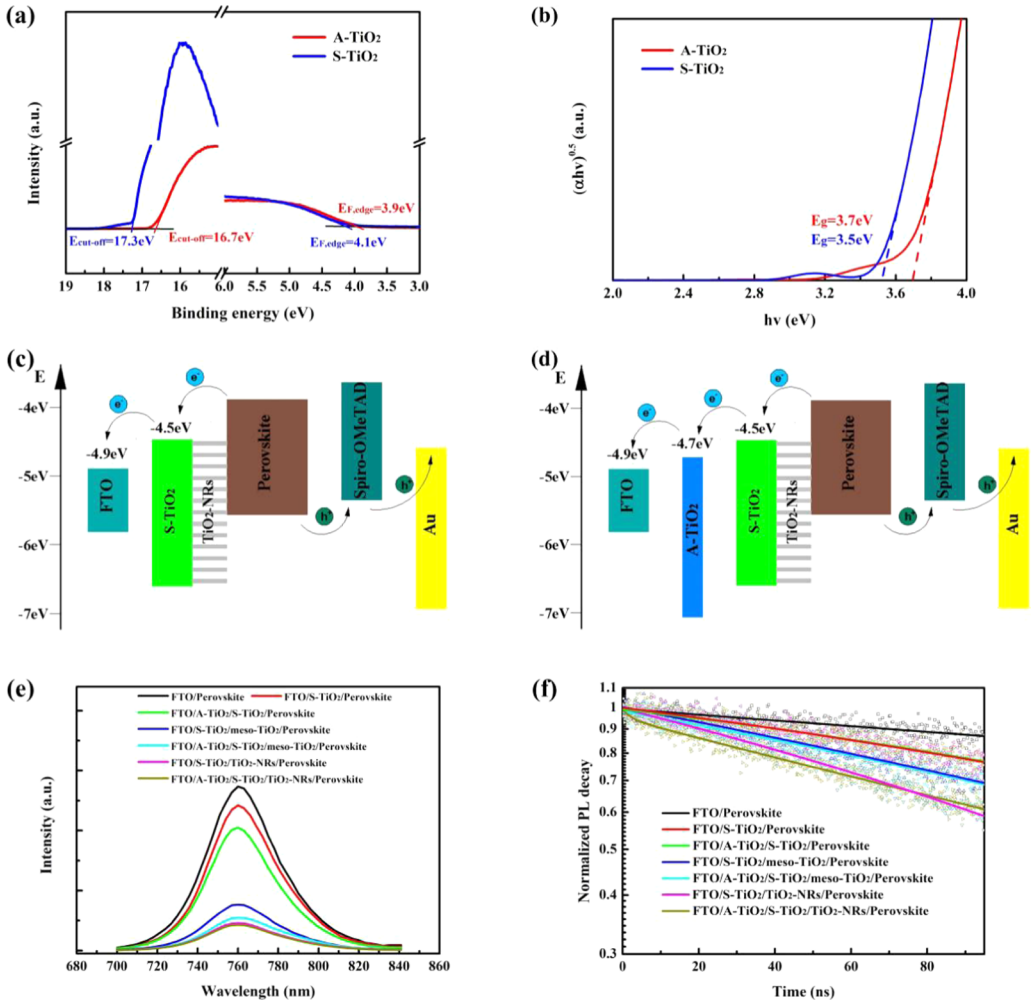

Figure 3. (a) UPS spectra of a A-TiO_2 layer (5 nm) and a S-TiO_2 layer (65 nm) with $E_{cut\text{-}off}$ and E_F, respectively. (b) Tauc plots with E_g of the A-TiO_2 layer and the S-TiO_2 layer. Energy levels of different layers in perovskite solar cells (c) without and (d) with the A-TiO_2 layer (5 nm). (e) Steady-state PL spectra and (f) TRPL decay of perovskite on different FTO/ETL combinations.

improved S-TiO_2 film quality enhances the charge transport,[38] which could partly account for the improved FF.

The A-TiO_2 can effectively inhibit the recombination between the FTO substrate and perovskite layers. To quantify the charge exchange between the working electrode and nearby electrolyte, cyclic voltammetry (CV) has been further applied to evaluate the charge recombination crossing the S-TiO_2 layer on the FTO substrate and on the FTO/A-TiO_2 substrate in aqueous $K_4Fe(CN)_6/K_3Fe(CN)_6$.[5] Figure 2c shows the CV curves of the redox couple at the S-TiO_2 film (65 nm) on FTO and the S-TiO_2 film on FTO/ A-TiO_2 (5 nm). The A-TiO_2 layer showed obvious blocking behavior by decreasing the intensity of anodic and cathodic peak current densities. The introduction of the A-TiO_2 layer allows reducing the interfacial recombination effectively, owing to the reduced physical contact defects at the FTO/S-TiO_2 interface and the reduced pinhole density within the S-TiO_2 layer. The results herein are in good agreement with the $J-V$ and EIS results.

To achieve high PCE values, it is of importance to tune the charge-selective layers to improve the charge extraction, transport, and collection. To shed light on the mechanism of charge extraction, the conduction band minimum (CBM) and work function (WF) values have been determined from the valence band maximum (VBM) values by ultraviolet photoelectron spectroscopy (UPS) and band gap (E_g) values through UV−vis absorption spectroscopy (Figure 3). The cutoff energies of A-TiO_2 and S-TiO_2 were 16.7 and 17.3 eV and the Fermi levels were 3.9 and 4.1 eV, respectively. Combined with the UV−vis results, the E_g values of A-TiO_2 and S-TiO_2 were determined as 3.7 and 3.5 eV, respectively. Therefore, the conduction band minima of A-TiO_2 and S-TiO_2 were calculated to be −4.7 and −4.5 eV, respectively. Previous studies showed that the CBM and VBM of TiO_2 NR are −4.19 and −7.33 eV, respectively.[33] Figure 3c,d shows the schematic drawings of the energy-level alignment in PSCs without/with the A-TiO_2 interlayer. Normally, due to the higher CBM position of the S-TiO_2, $E_{CBM\text{-}TiO2}$, than the work function of FTO (−4.9 eV), $W_{f\text{-}FTO}$,[60] the electrons from TiO_2 NRs and perovskite layer would be supposed to be injected from S-TiO_2 to FTO efficiently. It has been reported that electron injection occurs at the junction between FTO and compact TiO_2 in thermal equilibrium, when their Fermi levels show some differences prior to the materials being brought into contact.[61] Electron injection leads to an upbending of the compact TiO_2 and a depletion region at the FTO/TiO_2 interface, which causes electron accumulation within the compact TiO_2 layer and finally inhibits electron collection.[61] Herein, the energetic difference between $E_{CBM\text{-}TiO2}$ and $W_{f\text{-}FTO}$ is 0.4 eV, which

DOI: 10.1021/acsami.9b07610
ACS Appl. Mater. Interfaces 2019, 11, 33770−33780

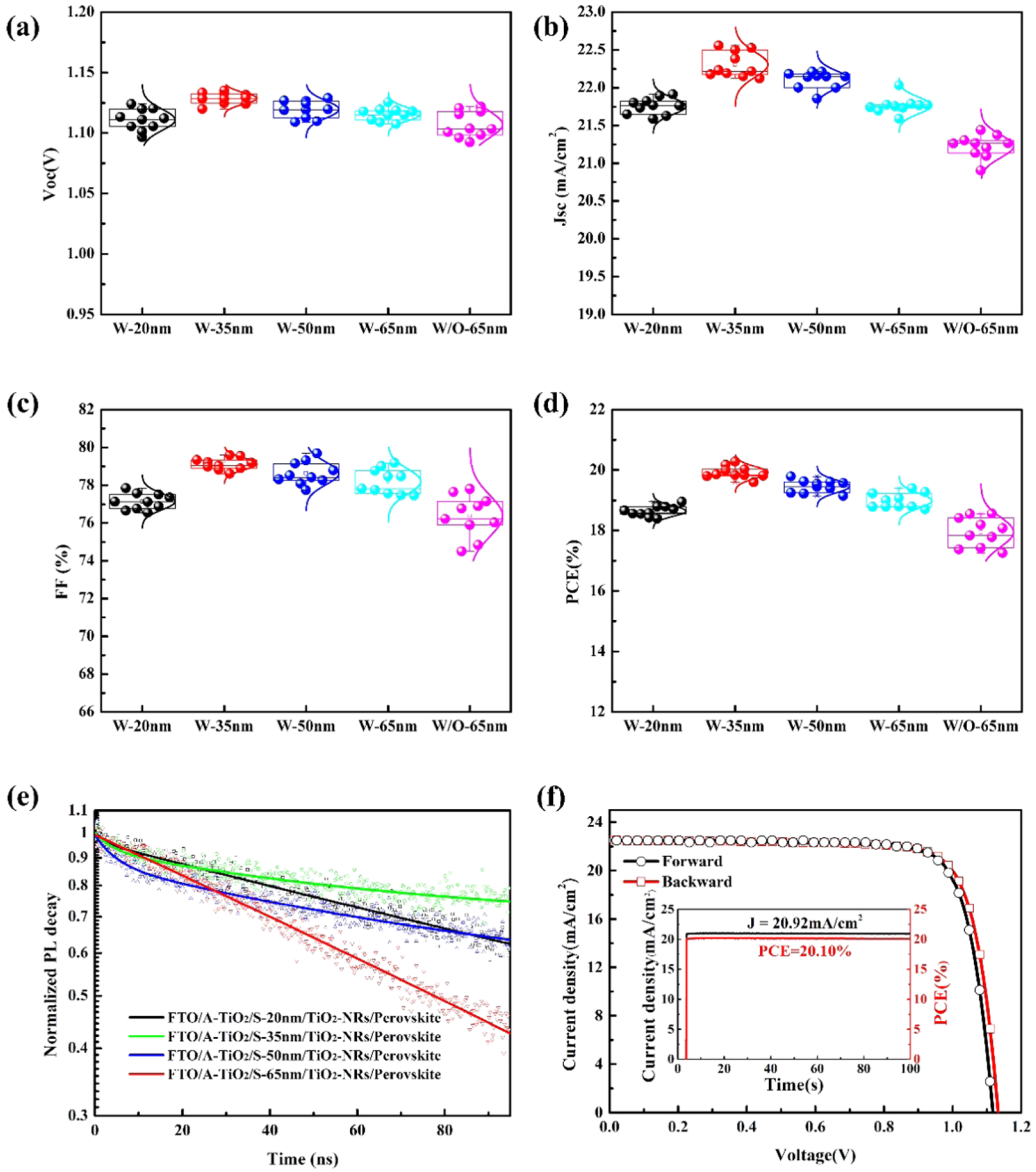

Figure 4. Photovoltaic characteristics of PSC devices. (a) Open-circuit voltage (V_{oc}), (b) short-circuit current (J_{sc}), (c) fill factor (FF), and (d) efficiency of devices based on S-TiO_2 layers with different thicknesses (20, 35, 50, and 65 nm). (e) TRPL decay for the perovskite films on different FTO/ETL combinations containing different S-TiO_2 layers with four thicknesses. (f) $J-V$ curve, steady-state current density, and efficiency of the best-performing cell based on FTO/A-TiO_2 (5 nm)/S-TiO_2 (35 nm)/perovskite film/spiro-OMeTAD/Au. The scan rate is 0.1 V s^{-1} for $J-V$ curves. The inset shows the steady-state photocurrent measurements at a voltage of 0.961 V.

might cause an energetic barrier between S-TiO_2 and FTO and then lower the charge extraction. The energy level of A-TiO_2 is well situated between S-TiO_2 and perovskite (Figure 3d). The A-TiO_2 thus enables the elimination of the energetic barrier between the S-TiO_2 layer and FTO, which accelerates remarkably the charge collection from the S-TiO_2 layer.

To verify the speedy electron collection, steady-state photoluminescence (PL) spectra of perovskite layers on different substrates have been recorded (Figure 3e). The PL intensity of the perovskite layer on the FTO/A-TiO_2/S-TiO_2/TiO_2 NR array was lower than that of the FTO/S-TiO_2/TiO_2 NR array, indicating the most efficient electron transport boosted by the insertion of the A-TiO_2 layer. The time-resolved photoluminescence (TRPL) decay has been monitored on perovskite layers on different substrates to elucidate the fast charge extraction (Figure 3f).[62] The modified FTO with the A-TiO_2 layer can help the charge decay from the perovskite layer. The TRPL lifetime decay can be fitted with a biexponential decay function containing a fast decay process and a slow decay process.[63] The fast decay process is regarded as the result of quenching of free carriers in the perovskite layer to ETL or HTL, while the slow decay process because of radiative decay is within the perovskite layer. For the structure of FTO/S-TiO_2/TiO_2 NR array/perovskite, the fast decay lifetime is 3.74 ns. Upon the addition of A-TiO_2 layer, the fast decay lifetime is decreased to 3.03 ns, thereby indicating that the A-TiO_2 layer enabled a faster electron extraction, leading to PL quenching that contributed to charge separation and collection in the FTO side. The results also confirmed the superiority of A-TiO_2 in accelerating charge extraction on different combinations of FTO/ETL/perovskite (Figure 3f). The details of the charge extraction are summarized in Table S2. Combined with the energetic analysis, the A-TiO_2 is

DOI: 10.1021/acsami.9b07610
ACS Appl. Mater. Interfaces 2019, 11, 33770−33780

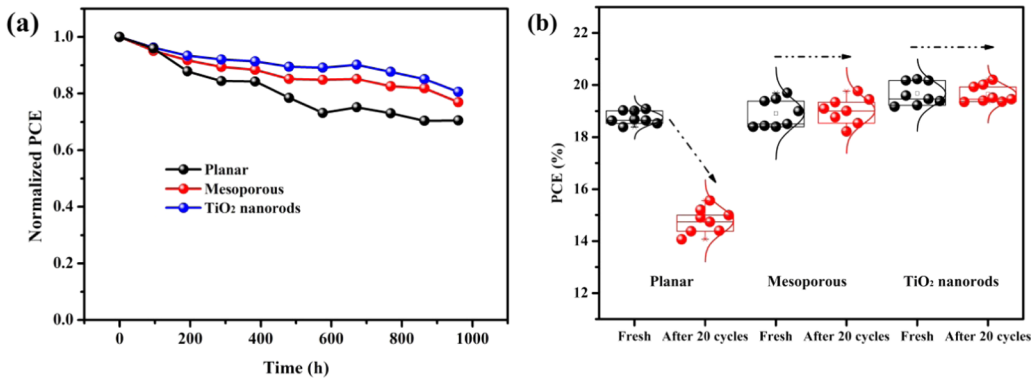

Figure 5. Dependence of normalized PCEs of SnO_2-based planar perovskite solar cells, mesoporous-TiO_2-based perovskite solar cells, and TiO_2-NR-based perovskite solar cells (a) on time at 85 °C in a N_2-filled container and (b) before and after 20 temperature cycles (−18 to 60 °C) in a N_2-filled container (herein, as-prepared devices and thermal-cycle-aged devices are denoted "Fresh" and "After 20 cycles", respectively). Before the *I*−*V* measurements, all of the cells were taken out of the containers and measured at room conditions. All of the cells are without encapsulation.

noticeably helpful for removing the energetic barrier along the FTO/S-TiO_2 junction to achieve high efficiency.

It has been showed that the thickness of the TiO_2 underlayer has a great effect on the efficiency and stability.[43,64,65] A thicker TiO_2 underlayer might increase the serial resistance and decrease the PCE.[66] Previously, we have revealed an optimal thickness of 65 nm for the S-TiO_2 layer[33,67] and hence the optimal thickness of the combination of A-TiO_2 and S-TiO_2 has to be determined. Thus, thickness dependence of S-TiO_2 based on FTO/A-TiO_2 has been further explored using the current−voltage (*I*−*V*) measurements. The current increases with the decrease in thickness, indicating the reduction of resistance (Figure S7). Although the decreased resistance is beneficial for the FF, the thinner compact layer might increase the risk of recombination.[37] CV measurements have indicated that the peak current density increases with the decreased S-TiO_2 layer thickness (Figure S7). Consequently, a balance should be reached between the decreased resistance of the A-TiO_2/S-TiO_2 layer on the FTO and the increased risk of back recombination. To achieve the optimal structure of the A-TiO_2/S-TiO_2 underlayer, different A-TiO_2/S-TiO_2 underlayers have been applied to TiO_2 NR array-based PSCs. The SEM images of the TiO_2 NR arrays grown on different underlayers indicated that the change of the S-TiO_2 thickness barely affects the morphology of TiO_2 NR arrays (Figure S8). To rule out the effect of the perovskite layer, X-ray powder diffraction (XRD) patterns have been monitored for perovskite layers prepared on the anodes with different A-TiO_2/S-TiO_2 underlayers (Figure S9). The changed S-TiO_2 shows almost no effect on the perovskite layer. Hence, the change of the S-TiO_2 thickness only accounts for the changed photovoltaic parameters of the PSCs (Figure 4, Table S3). In Figure 4, devices containing S-TiO_2 of 20, 35, 50, and 65 nm thicknesses on FTO/A-TiO_2 (5 nm) substrates are denoted W-20 nm, W-35 nm, W-50 nm, and W-65 nm, respectively. For comparison, devices based on FTO/S-TiO_2 (65 nm) are denoted W/O-65 nm. As shown in Figure 4a, the open-circuit voltage was almost not changed with the decreased S-TiO_2 thickness. Nevertheless, a too thin S-TiO_2 layer cannot effectively reduce the recombination and can lead to a slight decrease of V_{oc}. By reducing the thickness of S-TiO_2 from 65 to 35 nm, the current density increases initially and then decreases, owing to the effective charge collection for perovskite via the S-TiO_2 layer. Benefited from the less trap states within the layers, the thinner S-TiO_2 layer favors the charge transport and collection,[37] as confirmed by the TRPL decay results (Figure 4e). The details of the charge extraction lifetime are given in Table S2. The fast decay lifetime related to the charge extraction decreases with the thinner S-TiO_2 thickness, indicating a monotonically increasing charge collection efficiency. The change of FF consists the variation trend of the J_{sc} due to the decreased serial resistance of the S-TiO_2 layer via reducing the thickness. The best-performing PSCs can be achieved at the thickness of S-TiO_2 of around 35 nm.

The *J*−*V* curve of the champion cell using the optimized A-TiO_2 (5 nm)/S-TiO_2 (35 nm) underlayer has been measured for reverse and forward scan directions (Figure 4f). In the reverse scan, a J_{sc} of 22.50 mA cm^{-2}, V_{oc} of 1.13 V, and FF of 0.80 have been reached, yielding a PCE of 20.28%. Negligible hysteresis has been realized in this cell as the PCE from the forward scan (20.02%) was close to that from the reverse scan. To validate the J_{sc} measured under simulated sunlight, the external quantum efficiency (EQE) measurement for photocurrent generation has been performed to determine the J_{sc} (Figure S10).[68] The overall EQE values are larger than 80% throughout the UV−vis region, yielding a J_{sc} of 20.91 mA cm^{-2}. This matches closely to the measured J_{sc}, confirming the match between the sum simulator and the AM 1.5 standard solar emission. It is worth mentioning that the PCE value herein, to the best of our knowledge, is superior to previously reported one-dimensional array-based PSCs. Moreover, the best-performing cell had a steady-state current of 20.92 mA cm^{-2} and a steady-state PCE of 20.10% (inset, Figure 4f).

Despite the high PCE, one major concern is whether PSCs are long-term stable for terrestrial applications. The air stability of the device without encapsulation is shown in Figure S11. The PCE of the device remained above 95% after 28 days of the atmospheric storage (humidity <20%). The stability of the TiO_2-NR-based PSCs against heat was also evaluated at 85 °C under a N_2 environment. Figure 5a shows that eight unsealed PSCs retained, on average, 80.5% of their initial PCE after storing for 1000 h in a N_2-filled container. The performances of eight SnO_2-based PSCs and eight TiO_2-based mesoporous PSCs were also tested for comparison. The former and the latter retained average values of 70.5 and 77% of their initial PCE after 1000 h, respectively. As mentioned above, the resistance of the PSCs against temperature cycling is extremely important for their future application under outdoor conditions. We evaluated the performance of eight unsealed TiO_2-NR-based PSCs experiencing 20 temperature cycles

DOI: 10.1021/acsami.9b07610
ACS Appl. Mater. Interfaces 2019, 11, 33770−33780

between −18 and 60 °C, which is much milder than the standards of the International Electrotechnical Commission (IEC) 61646. Eight SnO_2-based planar PSCs and eight TiO_2-based mesoporous PSCs were also tested (Figures 5b and S12). All TiO_2-NR-based PSCs and TiO_2-based mesoporous PSCs retained more than 90% of their initial performance after 20 temperature cycles. However, the SnO_2-based PSCs retained less than 80% of their initial performance. Overall, the TiO_2-NR-based PSCs showed an extraordinary long-term durability owing to its role in mechanical reinforcement at the perovskite/TiO_2 NR interface, which is of great interest for PSC in the transition from the laboratory to real-world deployment.[55,69]

CONCLUSIONS

In summary, we have introduced a 5 nm TiO_2 layer between FTO and the spin-coated TiO_2 compact layer for TiO_2 NR array-based PSCs through ALD. The deposited thin layer inhibited the charge recombination by optimizing the spin-coated TiO_2 compact layer and the FTO/S-TiO_2 interface. The inserted layer improved the charge collection efficiency by reducing the energetic barrier between the spin-coated compact layer and the FTO substrate. We have unraveled that the thickness of the spin-coated TiO_2 compact layer is critical for reducing the serial resistance and charge recombination. The modification of the FTO with the 5 nm TiO_2 layer for hole blocking and energetic engineering could dramatically enhance the cell performance. Our best-performing cell showed an efficiency as high as 20.28% with negligible hysteresis, a maximum-power-point efficiency of 20.10%, and a long-term stability up to 30 days under ambient conditions without encapsulation. To the best of our knowledge, this is the first time to demonstrate the superiority of TiO_2-NR-based PSCs facing dry heat and thermal cycling circumstances to date. These results provide important future direction toward understanding the role of interlayer engineering in commercializing low-cost and highly efficient perovskite solar cells. It also holds the promise to provide new paradigms for other electronic materials and their applications, such as SSDSCs, sensors, and betavoltaics, where the TiO_2 NR array film with a tuned seeding layer could be applied to ensure effective electron extraction.

EXPERIMENTAL SECTION

Materials. $NH_2CH{=}NH_2I$ (FAI) was prepared by reacting formamidine acetate and hydroiodic acid (57 wt % in H_2O). Similarly, CH_3NH_3Br (MABr) was prepared by reacting methylamine (30−33 wt % in ethanol, Aladdin) and hydrobromic acid (48 wt % in H_2O, J&K). The concrete experimental operations were referred to a previous report.[3] Lead(II) iodide (99.9985%) was purchased from Alfa Asear, and spiro-OMeTAD was purchased from Lumtec (Taiwan). All other materials were purchased from Sigma-Aldrich. All chemicals were used as received.

Deposition of the TiO_2 Thin Layer by the ALD Method. The FTO glasses were etched with Zn powder and 3 M HCl. Then, the etched FTO glasses were washed successively by sonicating in detergent, 0.3 M HCl, deionized water, acetone, and isopropanol. After drying in an electrical oven, the FTO glasses were treated in an UV/ozone cleaner for 15 min. Subsequently, a thin TiO_2 layer of several nanometers was deposited on the FTO surface by the ALD method (TFS 200, BeneqOy) using titanium(IV) chloride and water as precursors. For one cycle, the metal precursor was first pulsed for 200 ms and then the extra precursor was removed by a purge of N_2 for 1000 ms. Next, a H_2O pulse for 100 ms was introduced followed by a N_2 purge for 1500 ms. The reaction temperature was fixed at 200 °C. Every cycle contributed to 0.02−0.06 nm TiO_2 growth. Approximately, 1, 3, 5, and 7 nm-thick TiO_2 layer on the FTO surface can be obtained after 17, 51, 85, and 119 cycles of deposition, respectively.

Preparation of S-TiO_2 and TiO_2 Nanorod Arrays. The compact TiO_2 layer for the growth of TiO_2 NR arrays was deposited on pristine or FTO/A-TiO_2 surface by spin-coating the precursor solution. The thickness of S-TiO_2 can be controlled by adjusting the concentration of titanium isopropoxide in the precursor solutions. To obtain 65, 50, 35, and 20 nm-thick TiO_2 compact layers, 592, 444, 296, and 148 μL of titanium isopropoxide were added into a mixture solution (10 mL ethanol, 10 μL H_2O, and 10 μL of HCl (37% in H_2O)), respectively. The solutions were spin-coated on pristine/modified FTO glasses at 2000 rpm for 60 s. Then, the glasses were annealed at 450 °C for 60 min. The TiO_2 NR arrays were grown on the as-annealed S-TiO_2 layers according to our previous report.[51]

Fabrication of PSC. FAI (1 M), MABr (0.2 M), PbI_2 (1.1 M), and $PbBr_2$ (0.2 M) were dissolved in 1 mL mixed solution of DMF/DMSO = 4:1 (v:v). Then, 44.5 μL of 1.5 M CsI in DMSO and 44.5 μL of 1.5 M KI in DMSO was added to the mixed solution to achieve $K_{0.05}Cs_{0.05}(MA_{0.17}FA_{0.83})_{0.9}Pb(I_{0.83}Br_{0.17})_3$ precursor solution. The perovskite precursor solution was then spin-coated on the TiO_2 NR arrays in a two-step consecutive spin-coating at 3000 and 6000 rpm for 10 and 25 s, respectively. During the program, 200 μL of chlorobenzene was poured onto the substrate 3 s before the end of the second step. As-prepared films were put on the heating plate immediately and annealed at 100 °C for 1 h. After the substrates were cooled down to room temperature, a spiro-OMeTAD solution containing 72.3 mg of spiro-OMeTAD, 17.5 μL of Li-bis-(trifluoromethanesulfonyl) imide solution (520 mg/mL in acetonitrile), and 28.8 μL of 4-*tert*-butylpyridine was coated onto the perovskite layer at 5000 rpm for 30 s. Finally, 70 nm of Au was thermally evaporated on the substrates.

Stability Test. The preparation of TiO_2-based mesoporous devices followed a previous report,[4] and a device architecture of FTO/compact TiO_2/mesoporous TiO_2/perovskite/spiro-OMeTAD/Au was used. The preparation of SnO_2-based planar devices was referred to a previous work,[42] and a device architecture of FTO/SnO_2/perovskite/spiro-OMeTAD/Au was applied. All of the PSCs going through the stability tests below are without encapsulation.

For the thermal stability test, the PSCs were stored in a sealed container filled with N_2 and then kept at 85 °C in an oven for 1000 h. To avoid the degradation of the spiro-OMeTAD, 10 wt % of CuPc was blended in the spiro-OMeTAD layer. The PSCs were periodically taken out of the container and measured. For the temperature cycling test, the devices were also stored in the sealed container filled with N_2 first. The container was first kept in an oven at 60 °C for 10 min. Afterward, the container was equilibrated at 25 °C for 5 min and then kept in a refrigerator at −18 °C for 10 min. The container was taken out of the refrigerator and was also equilibrated at 25 °C for 5 min. A cycle was completed when the container was moved to the oven.

Characterization. X-ray diffraction (XRD) patterns were obtained using a Rigaku Ultima-IV X-ray diffractometer. Electrochemical impedance spectroscopy was measured on an electrochemical station (Chenhua, CHI 660D) in the dark. The morphologies of the different TiO_2 films and FTO were observed by atomic force microscopy (AFM, Veeco DI Multimode V) and field-emission scanning electron microscopy (SEM, Zeiss Sigma). The Raman spectra were obtained by a Raman spectrometer (IDSpec ARCTIC) with a 532 nm laser of 50 mW power. The transmittance (% *T*) curves were acquired by a UV−vis spectrophotometer (Cary 5000). The UPS spectra were measured using X-ray photoelectron spectroscopy (Thermo Scientific ESCALAB 250Xi) with a −5.0 V bias voltage. The PL spectra were obtained using a fluorescence spectrophotometer (Hitachi F7000) with an excitation wavelength of 510 nm. The cyclic voltammetry (CV) curves were recorded by an electrochemical station (Chenhua, CHI 660D, China) using an aqueous electrolyte consisting of 0.5 M KCl, 0.5 mM $K_4Fe(CN)_6$, and 0.5 mM $K_3Fe(CN)_6$ at a scan rate of 0.02 V s^{-1}. A Pt wire was used as a counterelectrode, while the reference electrode was a saturated calomel electrode, and the measurement was carried out

DOI: 10.1021/acsami.9b07610
ACS Appl. Mater. Interfaces 2019, 11, 33770−33780

under an N_2 atmosphere. The current density−voltage (J−V) curves were recorded by a solar simulator (Newport Oriel) with a digital source meter (Keithley 2420). Prior to the measurement, a standard silicon solar cell was used as the reference (012-2013, Pharos Technology). The active area for all solar cells was fixed with a metal mask (0.1 cm^2). The external quantum efficiency (EQE) spectra were recorded using a QEX10 solar cell quantum efficiency measurement system.

■ ASSOCIATED CONTENT

Supporting Information

The Supporting Information is available free of charge on the ACS Publications website at DOI: 10.1021/acsami.9b07610.

SEM images of TiO_2 NR arrays on different substrates; dependence of the ALD-deposited film thickness on the cycle numbers; details of photovoltaic parameters for perovskite solar cells with different structures; Nyquist plots of perovskite solar cells with different thickness of A-TiO_2; AFM images, Raman spectra, XRD diagrams, I−V curves, and CV curves of S-TiO_2 on different substrates; XRD diagrams of perovskite films on different substrates; details of long-term and thermal cycles stability for perovskite solar cells with different structures; EQE of perovskite solar cell; and details of TRPL decay data (PDF)

■ AUTHOR INFORMATION

Corresponding Authors

*E-mail: lixin01@xmu.edu.cn (X.L.).
*E-mail: maixianmin@foxmail.com (X.M.).
*E-mail: gaoq@ornl.gov (Q.G.).
*E-mail: zguo10@utk.edu (Z.G.).

ORCID

Xin Li: 0000-0003-2036-1367
Hu Liu: 0000-0003-3840-8135
Zhanhu Guo: 0000-0003-0134-0210

Author Contributions

The manuscript was written through contributions of all authors. All authors have given approval to the final version of the manuscript.

Notes

The authors declare no competing financial interest.

■ ACKNOWLEDGMENTS

We gratefully acknowledge support from the National Natural Science Foundation of China (U1505243), the funding from Fujian Province of China (2016H0036, JZ160404, and 2015J01064), and the funding from Qinghai Province of China (2017-ZJ-750). Gao was supported as part of the Fluid Interface Reactions, Structures and Transport (FIRST) Center, an Energy Frontier Research Center funded by the US Department of Energy, Office of Science, Office of Basic Energy Sciences. A portion of this research was conducted at the Center for Nanophase Materials Sciences, which is a DOE Office of Science User Facility.

■ REFERENCES

(1) Snaith, H. J. Present Status and Future Prospects of Perovskite Photovoltaics. *Nat. Mater.* **2018**, *17*, 372−376.
(2) Kojima, A.; Teshima, K.; Shirai, Y.; Miyasaka, T. Organometal Halide Perovskites as Visible-Light Sensitizers for Photovoltaic Cells. *J. Am. Chem. Soc.* **2009**, *131*, 6050−6051.
(3) Saliba, M.; Matsui, T.; Domanski, K.; Seo, J. Y.; Ummadisingu, A.; Zakeeruddin, S. M.; Correabaena, J. P.; Tress, W. R.; Abate, A.; Hagfeldt, A.; et al. Incorporation of Rubidium Cations into Perovskite Solar Cells Improves Photovoltaic Performance. *Science* **2016**, *354*, 206−209.
(4) Saliba, M.; Matsui, T.; Seo, J. Y.; Domanski, K.; Correabaena, J. P.; Nazeeruddin, M. K.; Zakeeruddin, S. M.; Tress, W.; Abate, A.; Hagfeldt, A.; et al. Cesium-Containing Triple Cation Perovskite Solar Cells: Improved Stability, Reproducibility and High Efficiency. *Energy Environ. Sci.* **2016**, *9*, 1989−1997.
(5) Lee, Y. H.; Luo, J.; Son, M. K.; Gao, P.; Cho, K. T.; Seo, J.; Zakeeruddin, S. M.; Grätzel, M.; Nazeeruddin, M. K. Enhanced Charge Collection with Passivation Layers in Perovskite Solar Cells. *Adv. Mater.* **2016**, *28*, 3966.
(6) Peng, J.; Wu, Y.; Ye, W.; Jacobs, D. A.; Shen, H.; Fu, X.; Wan, Y.; Duong, T.; Wu, N.; Barugkin, C.; et al. Interface Passivation Using Ultrathin Polymer−Fullerene Films for High-Efficiency Perovskite Solar Cells with Negligible Hysteresis. *Energy Environ. Sci.* **2017**, *10*, 1792−1800.
(7) Jiang, Q.; Zhang, L.; Wang, H.; Yang, X.; Meng, J.; Liu, H.; Yin, Z.; Wu, J.; Zhang, X.; You, J. Enhanced Electron Extraction Using SnO2 for High-Efficiency Planar-Structure HC(NH2)2PbI3-Based Perovskite Solar Cells. *Nat. Energy* **2017**, *2*, No. 16177.
(8) Shin, S. S.; Yeom, E. J.; Yang, W. S.; Hur, S.; Kim, M. G.; Im, J.; Seo, J.; Noh, J. H.; Seok, S. I. Colloidally Prepared La-Doped BaSnO3 Electrodes for Efficient, Photostable Perovskite Solar Cells. *Science* **2017**, *356*, 167−171.
(9) Zhao, J.; Deng, Y.; Wei, H.; Zheng, X.; Yu, Z.; Shao, Y.; Shield, J. E.; Huang, J. Strained Hybrid Perovskite Thin Films and Their Impact on the Intrinsic Stability of Perovskite Solar Cells. *Sci. Adv.* **2017**, *3*, No. eaao5616.
(10) Rong, Y.; Hu, Y.; Mei, A.; Tan, H.; Saidaminov, M. I.; Seok, S. I.; McGehee, M. D.; Sargent, E. H.; Han, H. Challenges for Commercializing Perovskite Solar Cells. *Science* **2018**, *361*, No. eaat8235.
(11) Jiang, Q.; Chu, Z.; Wang, P.; Yang, X.; Liu, H.; Wang, Y.; Yin, Z.; Wu, J.; Zhang, X.; You, J. Planar-Structure Perovskite Solar Cells with Efficiency beyond 21%. *Adv. Mater.* **2017**, *29*, No. 1703852.
(12) Wang, P.; Jiang, Q.; Zhao, Y.; Chen, Y.; Chu, Z.; Zhang, X.; Zhou, Y.; You, J. Synergistic Improvement of Perovskite Film Quality for Efficient Solar Cells via Multiple Chloride Salt Additives. *Sci. Bull.* **2018**, *63*, 726−731.
(13) Rolston, N.; Bush, K. A.; Printz, A. D.; Gold-Parker, A.; Ding, Y.; Toney, M. F.; McGehee, M. D.; Dauskardt, R. H. Engineering Stress in Perovskite Solar Cells to Improve Stability. *Adv. Energy Mater.* **2018**, *8*, No. 1802139.
(14) Rolston, N.; Printz, A. D.; Tracy, J. M.; Weerasinghe, H. C.; Vak, D.; Haur, L. J.; Priyadarshi, A.; Mathews, N.; Slotcavage, D. J.; McGehee, M. D.; Kalan, R. E.; Zielinski, K.; Grimm, R. L.; Tsai, H.; Nie, W.; Mohite, A. D.; Gholipour, S.; Saliba, M.; Grätzel, M.; Dauskardt, R. H. Effect of Cation Composition on the Mechanical Stability of Perovskite Solar Cells. *Adv. Energy Mater.* **2018**, *8*, No. 1702116.
(15) Watson, B. L.; Rolston, N.; Printz, A. D.; Dauskardt, R. H. Scaffold-Reinforced Perovskite Compound Solar Cells. *Energy Environ. Sci.* **2017**, *10*, 2500−2508.
(16) Wang, Z. K.; Liao, L. S. Doped Charge-Transporting Layers in Planar Perovskite Solar Cells. *Adv. Opt. Mater.* **2018**, *6*, No. 1800276.
(17) Yang, M. J.; Guo, R.; Kadel, K.; Liu, Y. Y.; O'Shea, K.; Bone, R.; Wang, X. W.; He, J.; Li, W. Z. Improved Charge Transport of Nb-Doped TiO2 Nanorods in Methylammonium Lead Iodide Bromide Perovskite Solar Cells. *J. Mater. Chem. A* **2014**, *2*, 19616−19622.
(18) Wu, M. C.; Chan, S. H.; Lee, K. M.; Chen, S. H.; Jao, M. H.; Chen, Y. F.; Su, W. F. Enhancing the Efficiency of Perovskite Solar Cells Using Mesoscopic Zinc-Doped TiO2 as the Electron Extraction Layer through Band Alignment. *J. Mater. Chem. A* **2018**, *6*, 16920−16931.
(19) Giordano, F.; Abate, A.; Correa Baena, J. P.; Saliba, M.; Matsui, T.; Im, S. H.; Zakeeruddin, S. M.; Nazeeruddin, M. K.; Hagfeldt, A.;

DOI: 10.1021/acsami.9b07610
ACS Appl. Mater. Interfaces 2019, 11, 33770−33780

Graetzel, M. Enhanced Electronic Properties in Mesoporous TiO2 via Lithium Doping for High-Efficiency Perovskite Solar Cells. *Nat. Commun.* **2016**, *7*, No. 10379.
(20) Yu, M.; Long, Y.; Sun, B.; Fan, Z. Recent Advances in Solar Cells Based on One-dimensional Nanostructure Arrays. *Nanoscale* **2012**, *4*, 2783−2796.
(21) Zhou, X.; Wang, Z.; Xia, X.; Shao, G.; Homewood, K.; Gao, Y. Synergistic Cooperation of Rutile TiO2 {002}, {101}, and {110} Facets for Hydrogen Sensing. *ACS Appl. Mater. Interfaces* **2018**, *10*, 28199−28209.
(22) Chen, C.; Wang, N.; Zhou, P.; San, H.; Wang, K.; Chen, X. Electrochemically Reduced Graphene Oxide on Well-Aligned Titanium Dioxide Nanotube Arrays for Betavoltaic Enhancement. *ACS Appl. Mater. Interfaces* **2016**, *8*, 24638−24644.
(23) Dong, J.; Zhao, Y.; Shi, J.; Wei, H.; Xiao, J.; Xu, X.; Luo, J.; Xu, J.; Li, D.; Luo, Y.; Meng, Q. Impressive Enhancement in the Cell Performance of ZnO Nanorod-Based Perovskite Solar Cells with Al-Doped ZnO Interfacial Modification. *Chem. Commun.* **2014**, *50*, 13381−13384.
(24) Gao, C.; Yuan, S.; Cao, b.; Yu, J. SnO2 Nanotube Arrays Grown via an in situ Template-Etching Strategy for Effective and Stable Perovskite Solar Cells. *Chem. Eng. J.* **2017**, *325*, 378−385.
(25) Tavakoli, M. M.; Prochowicz, D.; Yadav, P.; Tavakoli, R.; Saliba, M. Zinc Stannate Nanorod as an Electron Transporting Layer for Highly Efficient and Hysteresis-less Perovskite Solar Cells. *Eng. Sci.* **2018**, *3*, 48−53.
(26) Li, S.; Zhang, P.; Chen, H.; Wang, Y.; Liu, D.; Wu, J.; Sarvari, H.; Chen, Z. D. Mesoporous PbI2 Assisted Growth of Large Perovskite Grains for Efficient Perovskite Solar Cells Based on ZnO Nanorods. *J. Power Sources* **2017**, *342*, 990−997.
(27) Yu, F. D.; Han, G. S.; Tu, Y. J.; Roh, H. S.; Lee, J. K. Electron Extraction Mechanism in Low Hysteresis Perovskite Solar Cells Using Single Crystal TiO_2 Nanorods. *Sol. Energy* **2018**, *167*, 251−257.
(28) Lee, J.; Sin, D. H.; Moon, B.; Shin, J.; Kim, H. G.; Kim, M.; Cho, K. Highly crystalline low-bandgap polymer nanowires towards high-performance thick-film organic solar cells exceeding 10% power conversion efficiency. *Energy Environ. Sci.* **2017**, *10*, 247−257.
(29) Kim, H. S.; Lee, J. W.; Yantara, N.; Boix, P. P.; Kulkarni, S. A.; Mhaisalkar, S.; Gratzel, M.; Park, N. G. High Efficiency Solid-State Sensitized Solar Cell-Based on Submicrometer Rutile TiO2 Nanorod and CH3NH3PbI3 Perovskite Sensitizer. *Nano Lett.* **2013**, *13*, 2412−2417.
(30) Wang, X. D.; Li, Z. D.; Shi, J.; Yu, Y. H. One-Dimensional Titanium Dioxide Nanomaterials: Nanowires, Nanorods, and Nanobelts. *Chem. Rev.* **2014**, *114*, 9346−9384.
(31) Wu, W. Q.; Huang, F. Z.; Chen, D. H.; Cheng, Y. B.; Caruso, R. A. Solvent-Mediated Dimension Tuning of Semiconducting Oxide Nanostructures as Efficient Charge Extraction Thin Films for Perovskite Solar Cells with Efficiency Exceeding 16%. *Adv. Energy Mater.* **2016**, *6*, No. 1502027.
(32) Jiang, Q.; Sheng, X.; Li, Y.; Feng, X.; Xu, T. Rutile TiO2 Nanowire-Based Perovskite Solar Cells. *Chem. Commun.* **2014**, *50*, 14720−14723.
(33) Cui, Q.; Zhao, X.; Lin, H.; Yang, L.; Chen, H.; Zhang, Y.; Li, X. Improved Efficient Perovskite Solar Cells Based on Ta-doped TiO2 Nanorod Arrays. *Nanoscale* **2017**, *9*, 18897−18907.
(34) Li, Y.; Zhao, Y.; Chen, Q.; Yang, Y.; Liu, Y.; Hong, Z.; Liu, Z.; Hsieh, Y. T.; Meng, L.; Li, Y.; et al. Multifunctional Fullerene Derivative for Interface Engineering in Perovskite Solar Cells. *J. Am. Chem. Soc.* **2015**, *137*, 15540−15547.
(35) Zhou, H.; Chen, Q.; Li, G.; Luo, S.; Song, T. B.; Duan, H. S.; Hong, Z.; You, J.; Liu, Y.; Yang, Y. Interface Engineering of Highly Efficient Perovskite Solar Cells. *Science* **2014**, *345*, 542−546.
(36) Gao, Q.; Yang, S.; Lei, L.; Zhang, S.; Cao, Q.; Xie, J.; Li, J.; Liu, Y. An Effective TiO2 Blocking Layer for Perovskite Solar Cells with Enhanced Performance. *Chem. Lett.* **2015**, *44*, 624−626.
(37) Ke, W.; Fang, G.; Wang, J.; Qin, P.; Tao, H.; Lei, H.; Liu, Q.; Dai, X.; Zhao, X. Perovskite Solar Cell with An Efficient TiO2 Compact Film. *ACS Appl. Mater. Interfaces* **2014**, *6*, 15959−15965.
(38) Wang, P.; Shao, Z.; Ulfa, M.; Pauporté, T. Insights Into the Hole Blocking Layer Effect on the Perovskite Solar Cell Performance and Impedance Response. *J. Phys. Chem. C* **2017**, *121*, 9131−9141.
(39) Wu, Y.; Yang, X.; Chen, H.; Zhang, K.; Qin, C.; Liu, J.; Peng, W.; Islam, A.; Bi, E.; Ye, F.; et al. Highly Compact TiO2 Layer for Efficient Hole-Blocking in Perovskite Solar Cells. *Appl. Phys. Express* **2014**, *7*, No. 052301.
(40) Fakharuddin, A.; Schmidt-Mende, L.; Garcia-Belmonte, G.; Jose, R.; Mora-Sero, I. Interfaces in Perovskite Solar Cells. *Adv. Energy Mater.* **2017**, *7*, No. 1700623.
(41) Zhou, X.; Liu, R.; Sun, K.; Friedrich, D.; McDowell, M. T.; Yang, F.; Omelchenko, S. T.; Saadi, F. H.; Nielander, A. C.; Yalamanchili, S.; Papadantonakis, K. M.; Brunschwig, B. S.; Lewis, N. S. Interface Engineering of the Photoelectrochemical Performance of Ni-Oxide-Coated n-Si Photoanodes by Atomic-Layer Deposition of Ultrathin Films of Cobalt Oxide. *Energy Environ. Sci.* **2015**, *8*, 2644−2649.
(42) Tao, C.; Neutzner, S.; Colella, L.; Marras, S.; Ram, A.; Kandada, S.; Gandini, M.; De Bastiani, M.; Pace, G.; Manna, L.; et al. 17.6% Stabilized Efficiency in Low-Temperature Processed Planar Perovskite Solar Cells. *Energy Environ. Sci.* **2015**, *8*, 2365−2370.
(43) Kegelmann, L.; Wolff, C. M.; Omondi, C. A.; Lang, F.; Unger, E. L.; Korte, L.; Dittrich, T.; Neher, D.; Rech, B.; Albrecht, S. It Takes Two to Tango - Double-Layer Selective Contacts in Perovskite Solar Cells for Improved Device Performance and Reduced Hysteresis. *ACS Appl. Mater. Interfaces* **2017**, *9*, 17245−17255.
(44) Tavakoli, M. M.; Yadav, P.; Tavakoli, R.; Kong, J. Surface Engineering of TiO_2 ETL for Highly Efficient and Hysteresis-Less Planar Perovskite Solar Cell (21.4%) with Enhanced Open-Circuit Voltage and Stability. *Adv. Energy Mater.* **2018**, *8*, No. 1800794.
(45) Wang, D.; Wu, C.; Luo, W.; Guo, X.; Qu, B.; Xiao, L.; Chen, Z. ZnO/SnO_2 Double Electron Transport Layer Guides Improved Open Circuit Voltage for Highly Efficient $CH_3NH_3PbI_3$-Based Planar Perovskite Solar Cells. *ACS Appl. Energy Mater.* **2018**, *1*, 2215−2221.
(46) Li, J.; Zhang, Z.; Gao, H.; Zhang, Y.; Mao, Y. Effect of Solvents on the Growth of TiO2 Nanorods and Their Perovskite Solar Cells. *J. Mater. Chem. A* **2015**, *3*, 19476−19482.
(47) Mali, S. S.; Betty, C.; Patil, P.; Hong, C. K. Synthesis of a Nanostructured Rutile TiO2 Electron Transporting Layer via an Etching Process for Efficient Perovskite Solar Cells: Impact of the Structural and Crystalline Properties of TiO_2. *J. Mater. Chem. A* **2017**, *5*, 12340−12353.
(48) Mali, S. S.; Chang, S. S.; Hui, K. P.; Heo, J.; Chang, K. H.; et al. Ultrathin Atomic Layer Deposited TiO2 for Surface Passivation of Hydrothermally Grown 1D TiO_2 Nanorod Arrays for Efficient Solid State Perovskite Solar Cells. *Chem. Mater.* **2015**, *27*, 1541−1551.
(49) Qiu, J.; Qiu, Y.; Yan, K.; Zhong, M.; Mu, C.; Yan, H.; Yang, S. All-Solid-State Hybrid Solar Cells Based on a New Organometal Halide Perovskite Sensitizer and One-Dimensional TiO_2 Nanowire Arrays. *Nanoscale* **2013**, *5*, 3245−3248.
(50) Wang, X.; Zhang, Z.; Qin, J.; Shi, W.; Liu, Y.; Gao, H.; Mao, Y. Enhanced Photovoltaic Performance of Perovskite Solar Cells Based on Er-Yb Co-doped TiO_2 Nanorod Arrays. *Electrochim. Acta* **2017**, *245*, 839−845.
(51) Xin, L.; Dai, S. M.; Pei, Z.; Deng, L. L.; Xie, S. Y.; Qian, C.; Hong, C.; Ning, W.; Hong, L. Efficient Perovskite Solar Cells Depending on TiO_2 Nanorod Arrays. *ACS Appl. Mater. Interfaces* **2016**, *8*, 21358−21365.
(52) Yang, M.; Guo, R.; Kadel, K.; Liu, Y.; O'Shea, K.; Bone, R.; Wang, X.; He, J.; Li, W. Improved Charge Transport of Nb-Doped TiO_2 Nanorods in Methylammonium Lead Iodide Bromide Perovskite Solar Cells. *J. Mater. Chem. A* **2014**, *2*, 19616−19622.
(53) Zhang, X.; Bao, Z.; Tao, X.; Sun, H.; Chen, W.; Zhou, X. Sn-Doped TiO_2 Nanorod Arrays and Application in Perovskite Solar Cells. *RSC Adv.* **2014**, *4*, 64001−64005.
(54) Chen, L.; Wang, J. R.; Xie, L. Q.; Zhan, C.; Qiu, Z.; Zhou, J. Z.; Yan, J. W.; Mao, B. W.; Tian, Z. Q. Compact Layer Influence on Hysteresis Effect in Organic−Inorganic Hybrid Perovskite Solar Cells. *Electrochem. Commun.* **2016**, *68*, 40−44.

DOI: 10.1021/acsami.9b07610
ACS Appl. Mater. Interfaces 2019, 11, 33770−33780

(55) Feng, X.; Zhu, K.; Frank, A. J.; Grimes, C. A.; Mallouk, T. E. Rapid Charge Transport in Dye-Sensitized Solar Cells Made from Vertically Aligned Single-Crystal Rutile TiO_2 Nanowires. *Angew. Chem., Int. Ed.* **2012**, *51*, 2727−2730.
(56) Jonda, C.; Mayer, A. B. R.; Stolz, U.; Elschner, A.; Karbach, A. Surface Roughness Effects and Their Influence on the Degradation of Organic Light Emitting Devices. *J. Mater. Sci.* **2000**, *35*, 5645−5651.
(57) Song, S.; Kang, G.; Pyeon, L.; Lim, C.; Lee, G. Y.; Park, T.; Choi, J. Systematically Optimized Bilayered Electron Transport Layer for Highly Efficient Planar Perovskite Solar Cells (η = 21.1%). *ACS Energy Lett.* **2017**, *2*, 2667−2673.
(58) Kavan, L.; Tétreault, N.; Moehl, T.; Grätzel, M. Electrochemical Characterization of TiO_2 Blocking Layers for Dye-Sensitized Solar Cells. *J. Phy. Chem. C* **2014**, *118*, 16408−16418.
(59) Ohsaka, T.; Izumi, F.; Fujiki, Y. Raman Spectrum of Anatase, TiO_2. *J. Raman Spectrosc.* **1978**, *7*, 321−324.
(60) Ma, J.; Yang, G.; Qin, M.; Zheng, X.; Lei, H.; Chen, C.; Chen, Z.; Guo, Y.; Han, H.; Zhao, X.; et al. MgO Nanoparticle Modified Anode for Highly Efficient SnO_2-Based Planar Perovskite Solar Cells. *Adv. Sci.* **2017**, *4*, No. 1700031.
(61) Snaith, H. J.; Grätzel, M. The Role of a "Schottky Barrier" at an Electron-Collection Electrode in Solid-State Dye-Sensitized Solar Cells. *Adv. Mater.* **2006**, *18*, 1910.
(62) Stolterfoht, M.; Wolff, C. M.; Márquez, J. A.; Zhang, S.; Hages, C. J.; Rothhardt, D.; Albrecht, S.; Burn, P. L.; Meredith, P.; Unold, T.; Neher, D. Visualization and Suppression of Interfacial Recombination for High-Efficiency Large-Area Pin Perovskite Solar Cells. *Nat. Energy* **2018**, *3*, 847−854.
(63) Zhao, X.; Shen, H.; Zhang, Y.; Li, X.; Zhao, X.; Tai, M.; Li, J. F.; Li, J.; Li, X.; Lin, H. Aluminum Doped Zinc Oxide as Highly Stable Electron Collection Layer for Perovskite Solar Cells. *ACS Appl. Mater. Interfaces* **2016**, *8*, 7826−7833.
(64) Choi, J.; Song, S.; Hörantner, M. T.; Snaith, H. J.; Park, T. Well-Defined Nanostructured, Single-Crystalline TiO_2 Electron Transport Layer for Efficient Planar Perovskite Solar Cells. *ACS Nano* **2016**, *10*, 6029−6036.
(65) Im, J.-H.; Lee, C.-R.; Lee, J.-W.; Park, S.-W.; Park, N.-G. 6.5% Efficient Perovskite Quantum-Dot-Sensitized Solar Cell. *Nanoscale* **2011**, *3*, 4088−4093.
(66) Chen, W.; Wu, Y.; Yue, Y.; Liu, J.; Zhang, W.; Yang, X.; Chen, H.; Bi, E.; Ashraful, I.; Grätzel, M.; et al. Efficient and Stable Large-Area Perovskite Solar Cells with Inorganic Charge Extraction Layers. *Science* **2015**, *350*, 944−948.
(67) Li, X.; Yang, L.; Wang, X.; Mai, X.; Wang, C.; et al. Constructing Efficient Mixed-ion Perovskite Solar Cells Based on TiO2 Nanorod Array. *J. Colloid Interface Sci.* **2019**, *534*, 459−468.
(68) Tavakoli, M. M.; Tress, W.; Milić, J. V.; Kubicki, D.; Emsley, L.; Grätzel, M. Addition of Adamantylammonium Iodide to Hole Transport Layers Enables Highly Efficient and Electroluminescent Perovskite Solar Cells. *Energy Environ. Sci.* **2018**, *11*, 3310−3320.
(69) Fakharuddin, A.; Giacomo, F. D.; Palma, A. L.; Matteocci, F.; Ahmed, I.; Razza, S.; D'Epifanio, A.; Licoccia, S.; Ismail, J.; Carol, A. D.; Brown, T. M.; Jose, R. Vertical TiO2 Nanorods as a Medium for Stable and High-Efficiency Perovskite Solar Modules. *ACS Nano* **2015**, *9*, 8420−8429.

DOI: 10.1021/acsami.9b07610
ACS Appl. Mater. Interfaces 2019, 11, 33770−33780